

RESEARCH ARTICLE

Induction of apically mistrafficked epiregulin disrupts epithelial polarity via aberrant EGFR signaling

Bhuminder Singh^{1,2,*}, Galina Bogatcheva¹, Evan Krystofiak³, Eliot T. McKinley^{1,2}, Salisha Hill⁴, Kristie Lindsey Rose⁴, James N. Higginbotham¹ and Robert J. Coffey^{1,2,*}

ABSTRACT

In polarized MDCK cells, disruption of the tyrosine-based YXXΦ basolateral trafficking motif (Y156A) in the epidermal growth factor receptor (EGFR) ligand epiregulin (EREG), results in its apical mistrafficking and transformation *in vivo*. However, the mechanisms underlying these dramatic effects are unknown. Using a doxycycline-inducible system in 3D Matrigel cultures, we now show that induction of Y156A EREG in fully formed MDCK cysts results in direct and complete delivery of mutant EREG to the apical cell surface. Within 3 days of induction, ectopic lumens were detected in mutant, but not wild-type, EREG-expressing cysts. Of note, these structures resembled histological features found in subcutaneous xenografts of mutant EREG-expressing MDCK cells. These ectopic lumens formed *de novo* rather than budding from the central lumen and depended on metalloprotease-mediated cleavage of EREG and subsequent EGFR activity. Moreover, the most frequent EREG mutation in human cancer (R147stop) resulted in its apical mistrafficking in engineered MDCK cells. Thus, induction of EREG apical mistrafficking is sufficient to disrupt selective aspects of polarity of a preformed polarized epithelium.

This article has an associated First Person interview with the first author of the paper.

KEY WORDS: 3D Matrigel culture, Epidermal growth factor receptor, EGFR, Epiregulin, EREG, Epithelial polarity, Epithelial transformation, Protein trafficking

INTRODUCTION

Epithelia line the surface of most internal organs and body cavities and are most often organized as a single polarized monolayer. Polarized epithelial cells exhibit an asymmetric distribution of proteins and lipids between the apical and basolateral cell surfaces, which are separated by tight junctions (Martin-Belmonte and Mostov, 2008). Since epithelia are continuously exposed to external deleterious factors and have a high proliferative potential, it is perhaps not surprising that more than 90% of cancers arise from this tissue. The epidermal growth factor (EGF) receptor (EGFR) is a

critical signaling hub for the establishment and maintenance of apico-basolateral polarity (Lof-Ohlin et al., 2017). EGFR is largely localized to the basolateral surface of polarized epithelial cells, which is dependent on distinct cytoplasmic juxtamembrane basolateral sorting motifs (Hobert and Carlin, 1995; Hobert et al., 1997; Vermeer et al., 2003). However, a small pool of apical EGFRs also exists with different signaling properties to basolateral EGFR (Kuwada et al., 1998; Singh et al., 2013). Dysregulated EGFR signaling is a hallmark of many cancers. In some cases, mutations and amplifications result in constitutive EGFR activation (Arteaga and Engelman, 2014), but, in most cancers, like in normal cells, EGFR activation depends on one of the seven mammalian EGFR ligands binding to EGFR (Harris et al., 2003). These ligands are synthesized as type I transmembrane precursors that are cleaved within the extracellular domain by metalloproteases to release a soluble ligand form that then binds to and activates EGFR (Singh and Coffey, 2014).

Five of the seven EGFR ligands studied are localized to the basolateral surface, which depends on their distinct basolateral sorting motifs (Dempsey et al., 2003; Dempsey et al., 1997; Gephart et al., 2011; Groenestege et al., 2007; Singh et al., 2015; Singh et al., 2013). Disruption of the basolateral sorting motifs in TGF- α (TGFA), amphiregulin (AREG), and betacellulin (BTC) lead to their nonpolarized distribution in polarized MDCK cells. However, EREG is markedly different as a single amino acid substitution (Y156A) in the YXXΦ basolateral sorting motif of EREG redirects it entirely to the apical surface (Singh et al., 2013). Moreover, when injected into the flanks of athymic nude mice, MDCK cells expressing mutant EREG formed locally invasive tumors that were seven-fold larger than MDCK cells expressing wild-type EREG (Singh et al., 2013). However, mechanism(s) underlying these striking effects are unknown.

The present study was designed to more directly assess the role of apical mistrafficking of EREG in these events. By inducing expression of basolateral-directed wild-type and apical-directed (Y156A mutant) EREG in fully formed polarized cysts of MDCK cells growing in 3D Matrigel, we show that expression of mutant EREG is sufficient to rapidly disrupt selected aspects of epithelial polarity, namely, formation of ectopic lumens and apical protrusions. Of note, these morphological abnormalities are observed in tumor xenografts of mutant EREG-expressing MDCK cells. We also show these effects are dependent on metalloprotease activity and EGFR signaling.


RESULTS

Biosynthesis and processing of basolateral WT and apical mutant Y156A EREG

To begin to understand the mechanism(s) underlying the dramatic effects associated with EREG apical mistrafficking, we first elected to compare the biosynthesis and processing of wild-type (WT) and Y156A mutant EREG by employing metabolic labeling and

¹Department of Medicine, Vanderbilt University Medical Center, Nashville, TN 37232, USA. ²Epithelial Biology Center, Vanderbilt University Medical Center, Nashville, TN 37232, USA. ³Cell Imaging Shared Resource, Cell and Developmental Biology, Vanderbilt University School of Medicine, Nashville, TN 37232, USA. ⁴Department of Biochemistry, Vanderbilt University, Nashville, TN 37232, USA.

*Authors for correspondence (robert.coffey@vmc.org; bhuminder.singh@vmc.org)

 B.S., 0000-0003-1357-2158; S.H., 0000-0002-4145-969X; R.J.C., 0000-0002-2180-3844

Handling Editor: Andrew Ewald

Received 21 October 2020; Accepted 9 August 2021

pulse-chase experiments. EREG-expressing polarized MDCK cells were pulse labeled for 20 min and chased with cold medium (Fig. 1A,B). As depicted in the schematic in Fig. 1C, both WT and Y156A mutant EREG–EGFP are synthesized as a ~44 kDa nascent polypeptide (isoform 1) to which a mannose-rich 14-sugar oligosaccharide is added at asparagine 47 (N47) within 20 min in the ER–Golgi secretory pathway, leading to its increased molecular mass (~72 kDa) (isoform 2); accumulation of form 2 is faster for WT EREG (Singh et al., 2013). During the ensuing 20 min, extraneous sugars are removed from the glycosylated precursor, which is then converted into a mature glycosylated cell surface form with a lower molecular mass of ~55 kDa as previously reported (isoform 3; Singh et al., 2013). This surface form is then cleaved by metalloproteases over the next 1–2 h to release the soluble EREG peptide (green, ~6 kDa), leaving a membrane-embedded EGFP-tagged remnant (isoform 4) that contains the EREG transmembrane and cytoplasmic domains (~35 kDa).

Metalloprotease sensitivity of EREG was next tested with a broad-spectrum metalloprotease inhibitor, galardin. Preincubation of EREG–EGFP-expressing cells with galardin led to accumulation of higher molecular mass forms (55 kDa) and disappearance of the 38 kDa band, showing that EREG is constitutively cleaved by metalloproteases (Fig. S1). It also confirmed that the chimeric protein is biologically active and that the 55 kDa form contains the extracellular EGF domain, which the metalloprotease cleaves from the transmembrane precursor. Combined, these results indicate that although transit of Y156A EREG through the secretory pathway is modestly delayed, both WT and Y156A EREG undergo similar biosynthetic processing, leading to formation of cell surface forms that are substrates for metalloprotease cleavage.

Apically mistrafficked EREG is associated with ectopic lumens in MDCK cysts

To examine the effect of EREG mistrafficking on polarity, we first elected to study MDCK cells constitutively expressing EREG in 3D Matrigel cultures. When grown as a single-cell suspension in Matrigel, MDCK cells formed cysts with a single central lumen that is lined by an inward facing apical surface and a basolateral surface facing outwards in contact with the Matrigel (Fig. 2, top panels). WT EREG expression led to formation of larger MDCK cysts, consistent with its growth-promoting properties, but the overall architecture was maintained (Fig. 2, middle panels). In contrast, mutant Y156A EREG expression led to even larger MDCK cysts with structural irregularities, ectopic lumens and luminal protrusions (Fig. 2, bottom panels). Ectopic lumens and inward growth were also observed histologically in nude mouse xenografts of MDCK cells expressing (Y156A)EREG–EGFP (Fig. S2). These characteristics have been observed previously with oncogenic perturbations of breast epithelial MCF-10A and MDCK Matrigel cultures, and have been touted as being *in vitro* surrogates for transformation (Aranda et al., 2006; Li et al., 2014; Simian and Bissell, 2017). Thus, stably expressing apically mistrafficked Y156A EREG in MDCK cells in 3D leads to altered polarity with structural features resembling those observed when these cells form tumors *in vivo*.

Induction of apically mistrafficked EREG increases the number of ectopic lumens formed in MDCK cysts

Thus far, we have studied MDCK cells constitutively expressing WT or Y156A EREG–EGFP. To more directly link apical mistrafficking of mutant EREG to disruption of polarity and a transformed phenotype, we generated doxycycline-inducible WT- or Y156A- EREG–EGFP-expressing MDCK cells. Single-cell

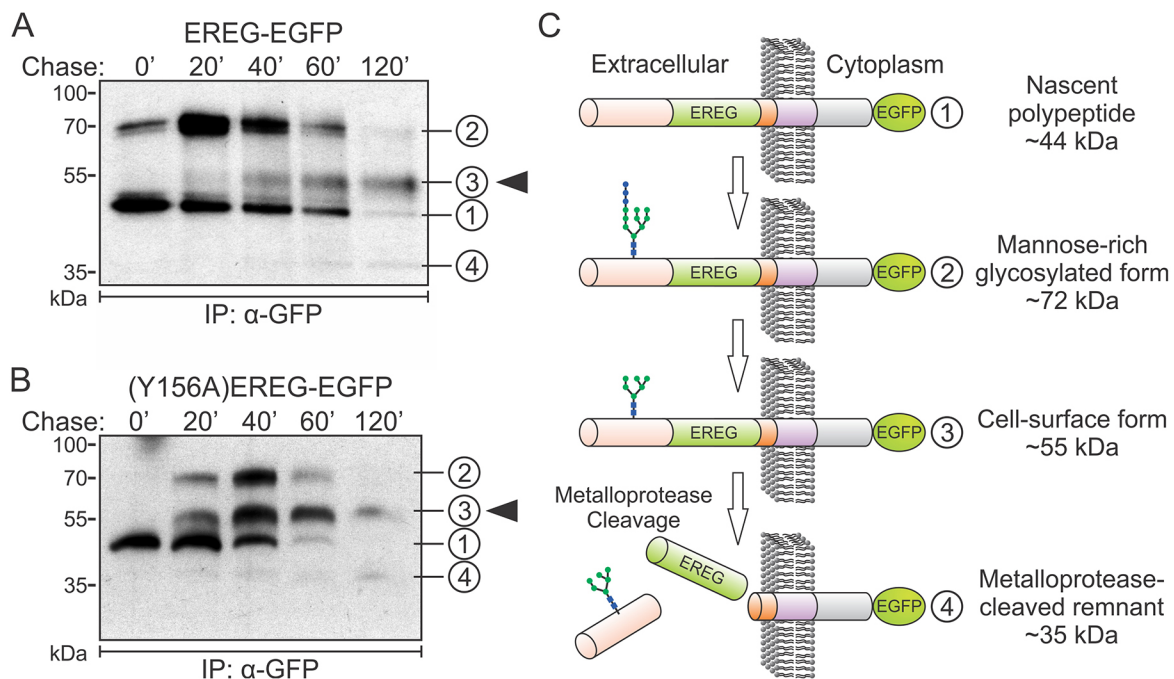


Fig. 1. Biosynthesis and processing of basolateral WT and apical mutant EREG. MDCK cells stably expressing (A) WT EREG–EGFP and (B) (Y156A)EREG–EGFP were polarized on Transwell filters and pulse-labeled (20 min) and chased for indicated times (minutes). After pulse-chase, cells were lysed, immunoprecipitated with GFP antibody, resolved on SDS-PAGE (8–12% gradient) gels, dried, and autoradiographs were developed. Bands representing EREG biosynthetic intermediates are numbered and matched in schematic in C. Arrowhead indicates cell-surface form. Images are representative of three repeats. (C) EREG biosynthesis and post-translational processing: summary of pulse-chase experiments from A and B. Major EREG biosynthetic intermediates observed in A and B are indicated as 1, 2, 3 and 4, and correspond to the numbers in the schematic. EREG domain organization: pro-region (pink), mature EREG region (light green) and transmembrane domain (purple); EGFP was fused to the C-terminus of full-length human EREG.

suspensions of these two clones were seeded into Matrigel and allowed to grow for 3 days, at which time they both formed small cysts with distinct apical and basolateral surfaces. A single dose of doxycycline was then given to induce expression of WT or Y156A EREG–EGFP (Fig. 3A). We optimized doxycycline doses to achieve comparable expression of WT (500 ng/ml) and Y156A (125 ng/ml) EREG. Parental MDCK Matrigel cultures were indistinguishable from each other under the uninduced and induced conditions; the population distribution of cyst diameters remained unchanged (Fig. 3B, top panel; Table S1). Induction of WT EREG led to a shift in the population to cysts with a larger diameter (Fig. 3B, middle panel), with mean cyst diameter increasing from 53 μ m to 64 μ m (Table S1). Induction of Y156A EREG also led to an increase in mean cyst diameter from 49 μ m to 62 μ m (Fig. 3B, lower panel, Table S1), which was significantly different from uninduced conditions. We next examined cysts at the individual level. After 5 days of culture (2 days after induction), basolateral localization of WT EREG–EGFP (Fig. 3C, second row) and apical localization of (Y156A)EREG–EGFP were observed (Fig. 3C, third row). At this stage both WT and Y156A EREG-expressing MDCK cysts showed normal epithelial polarity with normal localization of the apical marker gp135 (also known as PODXL) and tight junction marker ZO-1 (also known as TJP1).

When (Y156A)EREG–EGFP expression was allowed to continue until 7 days of culture, we observed formation of multiple ectopic lumens, in addition to the central lumen in MDCK cysts. Along with analyzing single images at the equatorial cyst planes (Fig. 3C), we performed 3D reconstructions of entire cysts from multiple confocal images (Fig. 3D; Movie 1) to show that the ectopic lumens are physically separate from the central lumen in (Y156A)EREG–EGFP-expressing cysts. Here, only gp135 and ZO-1 are included to highlight apical luminal structures and to eliminate obstruction by GFP and DAPI layers. When quantified, more than 13 cysts per low magnification field of view (10 \times objective) exhibited ectopic lumens

in (Y156A)EREG–EGFP-expressing MDCK Matrigel cultures; parental and EREG–EGFP-expressing MDCK cultures had about two cysts with ectopic lumens under similar conditions (Fig. 3E; Table S2).

Mutant EREG-induced ectopic lumens retain epithelial junctions, microvilli and primary cilia

We next performed transmission electron microscopy (TEM) of MDCK cysts expressing EREG–EGFP or (Y156A)EREG–EGFP as shown in Fig. 4A. Here, we observed that the central lumen for both WT and Y156A EREG expressing cysts had microvilli and that these central lumens were surrounded by cell–cell adhesions, such as tight junctions and adherens junctions (Fig. 4A, upper right magnified panel). Y156A EREG-expressing cysts, however, also had ectopic lumens, which were associated with microvilli and surrounding tight junctions and adherens junctions (Fig. 4A, lower right magnified panel). Additionally, primary cilia, another specialized apical structure, were observed in parental and WT EREG-expressing cysts (Fig. 4B, insets). Primary cilia were also observed within ectopic lumen in Y156A EREG-expressing cysts (Fig. 4B, bottom row). We also examined whether sorting of basolateral proteins was altered in the presence of ectopic lumens; we observed that basolateral proteins like Na⁺/K⁺-transporting ATPase α 1 subunit (ATP1A1) and p120 catenin (CTNND1) were excluded from the central and ectopic lumens (Fig. S3). Thus, inducible expression of mutant EREG results in a temporal disruption of selected aspects of epithelial polarity as manifested by ectopic lumen formation. Combined results from Fig. 4 and Fig. S3 indicate that ectopic lumens are mature apical structures complete with primary cilia and microvilli that are limited by cell–cell junctions.

Ectopic lumens form *de novo* and are dependent on metalloprotease activity and EGFR signaling

While central lumen formation of MDCK cysts in Matrigel cultures is well-studied, the formation of ectopic lumens is not (Bernascone et al., 2017; Martin-Belmonte and Mostov, 2008; Schluter and Margolis, 2009). We followed WT and Y156A EREG-expressing MDCK cysts after doxycycline induction by imaging every 40 min for 3 days after allowing cysts to form for an initial 3 days. We observed the characteristic spinning of MDCK cysts after induction of WT EREG; EREG basolateral localization was maintained as well as a single central lumen during the 3 days of imaging (Fig. 5, top panels; Movie 2) (Wang et al., 2013). However, when we observed the MDCK cysts induced for Y156A EREG expression, we observed an appearance of apical EREG–EGFP fluorescence and noticed that cyst spinning appeared to be compromised (Fig. 5, bottom panels; Movie 2). An ectopic lumen (arrow) that was observed towards the end of the 3 days of live imaging appeared at a site away from the central lumen without any connection with the central lumen at any time during the imaging window (Fig. 5, bottom panels; Movie 2). Thus, ectopic lumens appear to form *de novo* without budding from a central lumen.

We next hypothesized that EREG mistrafficking to the apical surface alone may not be sufficient for ectopic lumen formation but that its cleavage to release soluble ligand that then binds and activates EGFR is required (schematic Fig. 6A). Upon treatment with the broad-spectrum metalloprotease inhibitor BB-94, which inhibits EREG cleavage, we observed that induction of ectopic lumens by Y156A EREG was abrogated (Fig. 6B, central panels); BB-94 and doxycycline were added at day 3 and cysts were imaged at day 6. Similarly, addition of the irreversible EGFR inhibitor EKI-785 at the time of Y156A EREG induction compromised formation

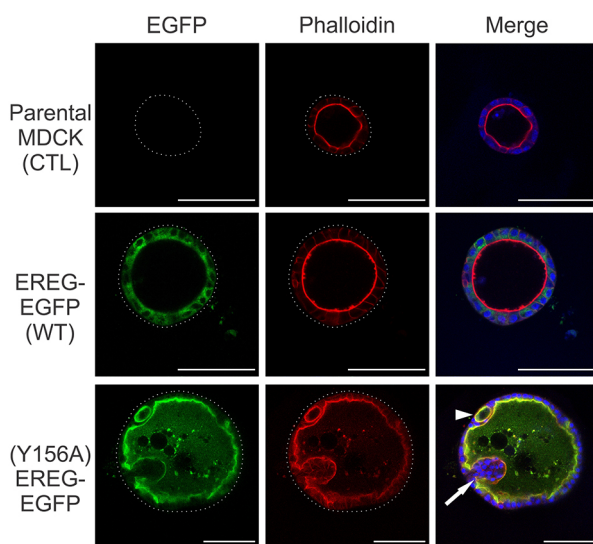


Fig. 2. Apically mistrafficked EREG leads to ectopic lumen formation in MDCK cysts. MDCK cells stably expressing indicated EREG constructs were cultured in Matrigel for 7 days. Cysts were then fixed and stained with phalloidin (red) and DAPI (blue). Cysts imaged at the equatorial plane are shown; EREG–EGFP fluorescence is depicted in green. Dotted white lines highlight cyst outer margins. Arrow and arrowhead in the bottom panel indicate luminal invagination and ectopic lumen, respectively, of a (Y156A)EREG–EGFP cyst. Images are representative of three repeats. Scale bars: 100 μ m.

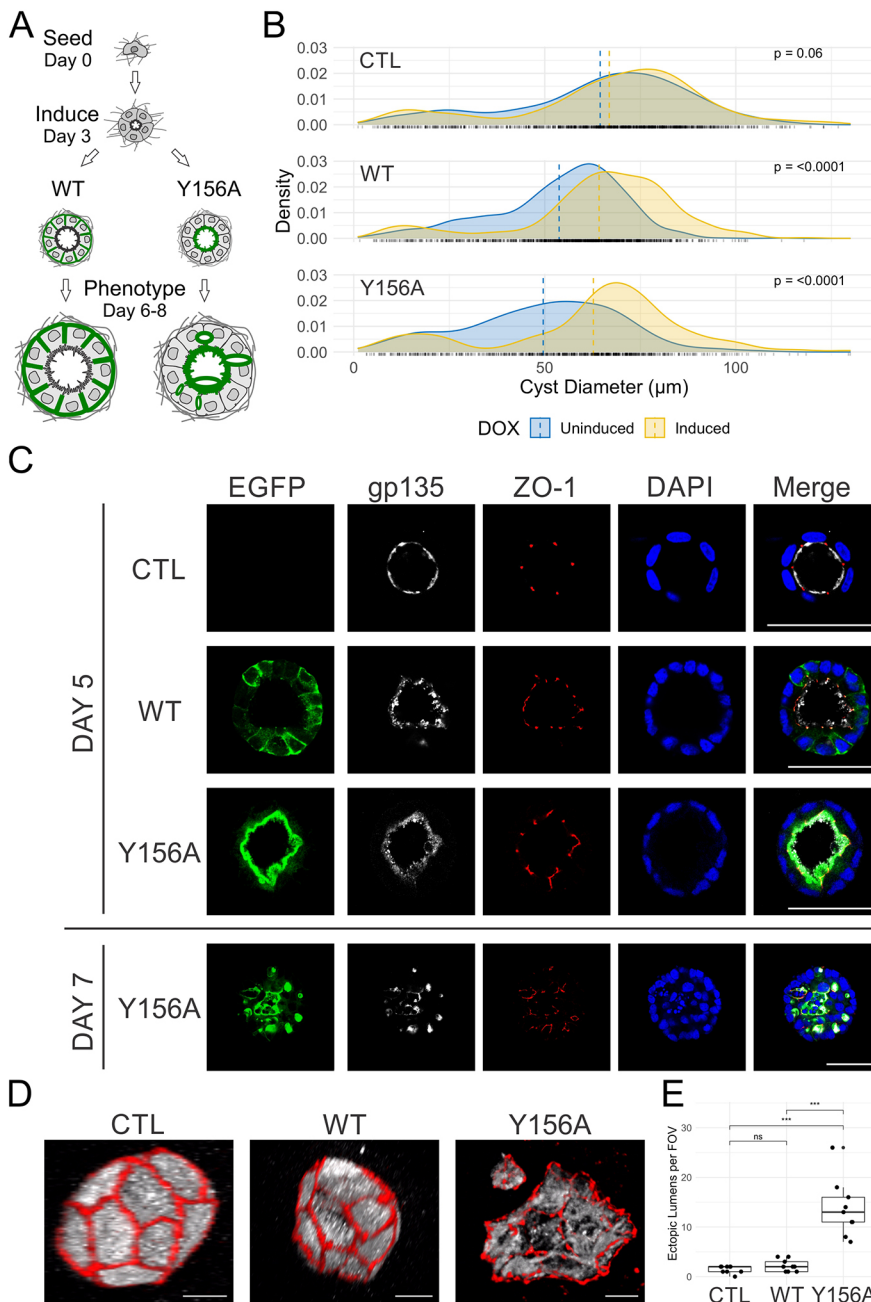


Fig. 3. Induction of apically mistrafficked EREG increases MDCK ectopic lumens.

(A) EREG induction after MDCK cyst formation using the doxycycline-inducible system. MDCK cells were seeded as single-cell suspension in Matrigel and allowed to grow for 3 days to allow cell division and cyst formation. A single doxycycline dose was then added to induce WT or Y156A EREG–EGFP expression and cells were maintained for another 3–5 days.

(B) 7-day-old MDCK Matrigel cultures with WT and Y156A mutant EREG–EGFP induced at day 3 were stained, imaged, and quantified for cyst diameters. Dotted vertical lines indicate average cyst diameters.

(C) Cysts expressing WT or Y156A EREG–EGFP constructs induced at day 3 and fixed at day 5 or 7 as indicated. After fixing, cysts were stained for gp135 (white), ZO-1 (red) and nuclei (DAPI, blue), and imaged at the equatorial plane; EREG–EGFP fluorescence is depicted in green. Images are representative of three repeats. Scale bars: 50 μm .

(D) 3D reconstruction of apical regions stained with gp135 (white) and ZO-1 (red) of cysts expressing WT or Y156A EREG–EGFP constructs as indicated to highlight ectopic lumens (full 360° view in Movie 1). Images are representative of three repeats. Scale bars: 10 μm .

(E) Number of cysts expressing indicated EREG constructs that contain ectopic lumens per low-magnification (10× objective) field of view (FOV) is depicted as a box plot with median indicated with horizontal line within the interquartile range box. Whiskers extend to the maximum and minimum values that are within 1.5 times the interquartile range, beyond which the ‘outlying’ points are plotted individually. Dots represent individual FOVs. Ns, not significant ($P > 0.05$); *** $P < 0.001$ (Wilcoxon rank sum test).

of ectopic lumens at 6 days (Fig. 6B, right panels). Nearly 90% of Y156A-expressing MDCK cysts exhibited multiple lumens. Addition of BB-94 and EKI-785 led to a significant reduction in the fraction of cysts with ectopic lumens (Fig. 6C). We also show that induction of apically mistrafficked EREG stimulates EGFR phosphorylation in polarized MDCK cells cultured on Transwell filters (Fig. S4A), and that cleavage of this mutant is inhibited by the metalloprotease inhibitors galardin and BB-94 (Fig. S4B). Combined, these data indicate that cleavage of apically mistrafficked EREG and subsequent EGFR activation is required for the formation of ectopic lumens.

The most abundant EREG cancer-associated mutation, R147stop, leads to its apical mistrafficking

We next tested whether EREG mistrafficking occurs in human cancer. We found that the most abundant human cancer mutation for

EREG in the Cbioportal database was R147stop (R147*), which removes the Y156-containing downstream basolateral-sorting motif (Fig. 7A,B) (Gao et al., 2013; Singh et al., 2013). We expressed this mutation as the EGFP chimera (R147*)EREG–EGFP and stably expressed it in MDCK cells. By immunofluorescence, we observed that a majority of the chimera localized to the apical cell surface (Fig. 7C, left panel). We also tested this mutation by selective cell-surface biotinylation and observed that >90% of R147* EREG localized to the apical cell surface (Fig. 7C, middle panel). We next identified and procured a human breast cancer cell line, HDQ-P1, which harbors the EREG R147* mutation. HDQ-P1 cells also formed cysts with ectopic lumens in 3D Matrigel cultures (Fig. S5A), and their *in vitro* growth is dependent on active EGFR signaling (Fig. S5B). These results indicate that the EREG R147* mutation leads to its apical mistrafficking and support the clinical relevance of this work.

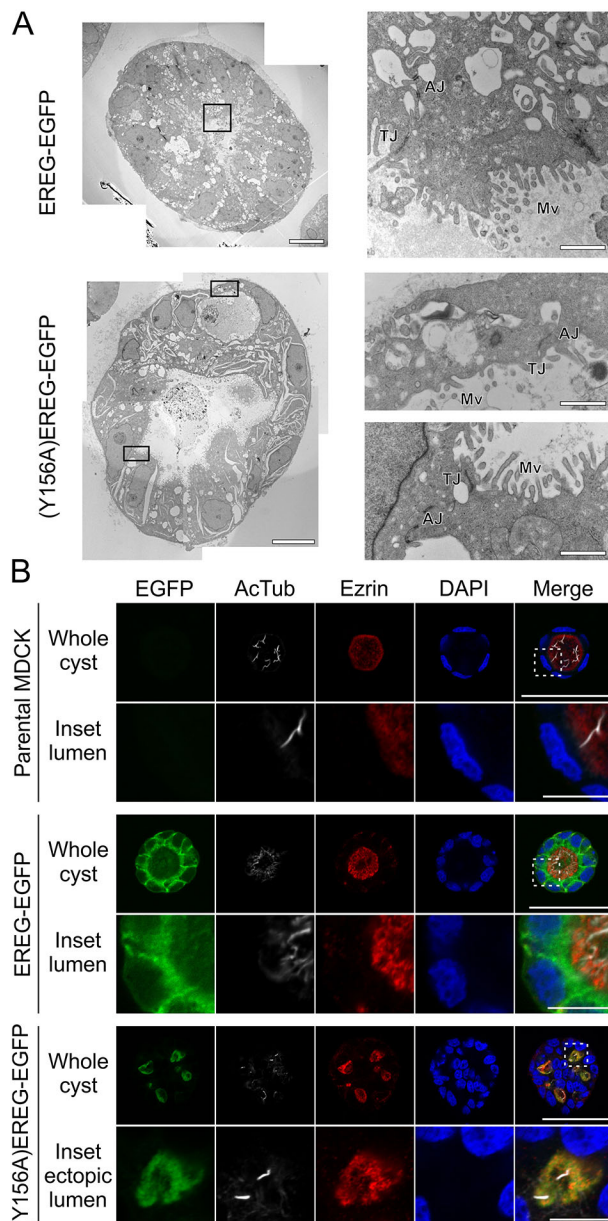


Fig. 4. EREG-induced ectopic lumens retain epithelial junctions, microvilli and primary cilia. (A) Representative MDCK cysts expressing indicated EREG constructs were fixed and processed for TEM. Full cysts are displayed on the left; regions highlighted with black borders are displayed at higher magnification on the right. For (Y156A)EREG–EGFP-expressing MDCK cysts, regions from both the ectopic lumen and central lumen are depicted in the magnification in upper and lower panels, respectively. TJ, tight junctions; AJ, adherens junctions; Mv, microvilli. Scale bars: 10 μ m (left panels); 500 nm (magnified panels on right). (B) MDCK cysts expressing the indicated EREG constructs were fixed and stained for the primary cilium [acetylated tubulin (AcTub), white], ezrin (red) and DNA (DAPI, blue). Images from cyst equatorial planes are displayed on top and highlighted luminal regions (dashed boxes) are displayed underneath at higher magnification. The bottom panels associated with (Y156A)EREG–EGFP show primary cilium staining (AcTub) in ectopic lumens. Images are representative of three repeats. Scale bars: 50 μ m (top panels); 10 μ m (magnified lower panels).

DISCUSSION

We previously showed that basolateral delivery of EREG was controlled by a single tyrosine residue (Y156) within its cytoplasmic domain and that a Y156A substitution completely

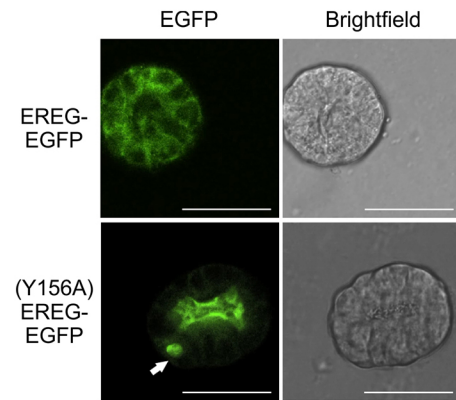


Fig. 5. Ectopic lumens form *de novo*. MDCK cysts were induced at day 3 to express EREG–EGFP or (Y156A)EREG–EGFP as indicated and followed over the next 3 days by live-cell imaging. Stills from the composite video (Movie 2) imaged at equatorial plane are displayed here from the time ectopic lumen (white arrow) first appear after induction of Y156A EREG expression. GFP fluorescence and brightfield channels are shown here. Images are representative of three repeats. Scale bars: 50 μ m.

redirected EREG to the apical surface, which was associated with transformation *in vitro* and *in vivo* (Singh et al., 2013). The present studies significantly extend these findings and provide mechanistic insight into these remarkable observations. Apically mistrafficked EREG induces a selective disruption of epithelial polarity in 3D (ectopic lumens), which is further dependent on EREG cleavage by metalloproteases and subsequent binding to activate EGFR. A multiple lumen phenotype has previously been shown to correlate with transformation in multiple 3D epithelial culture models and resembles features observed in MDCK nude mice xenografts expressing the apical Y156A mutant EREG (Aranda et al., 2006; Li et al., 2014; Simian and Bissell, 2017). We also show that the most common EREG human cancer mutation (R147*) results in its apical mistrafficking.

EREG biosynthesis and processing

WT and Y156A mutant EREG have similar modes of biosynthesis and processing as the sequence of label incorporation for both is for isoforms 1>2>3>4 (see bands labeled in Fig. 1A–C). Notably, the size difference between bands for isoforms 1 and 2 might not be completely explained by core glycosylation (14-sugar *en bloc* addition) as additional modifications like sialylation may be required (Bhide and Colley, 2017). Interestingly, EGFR also undergoes sialylation, which modulates EGFR activity in cancer cells (Britain et al., 2018). To unequivocally describe the sequence of events during EREG maturation, additional in-depth experiments like determining the Endo H sensitivity of major biosynthetic intermediates might be required.

Compared to WT, initial glycosylation of Y156A EREG appears to be slower (compare appearance of isoform 2 at 0 and 20 min timepoints in Fig. 1A,B). However, subsequent accumulation of the processed isoform 3 appears to be faster for Y156A EREG. After surface delivery, cleavage efficiency of WT and Y156A EREG is similar, as within 2 h of chase with cold medium the membrane remnant forms for both WT and Y156A EREG were observed (Fig. 1A,B). Also, under our experimental conditions, both basolateral and apical EREG are constitutively cleaved. It is interesting to speculate regarding the sources of apical EREG protease activity since the most-characterized EREG protease ADAM17 localizes to the basolateral surface (Merchant et al., 2008). Combined, these findings show that both the WT and Y156A

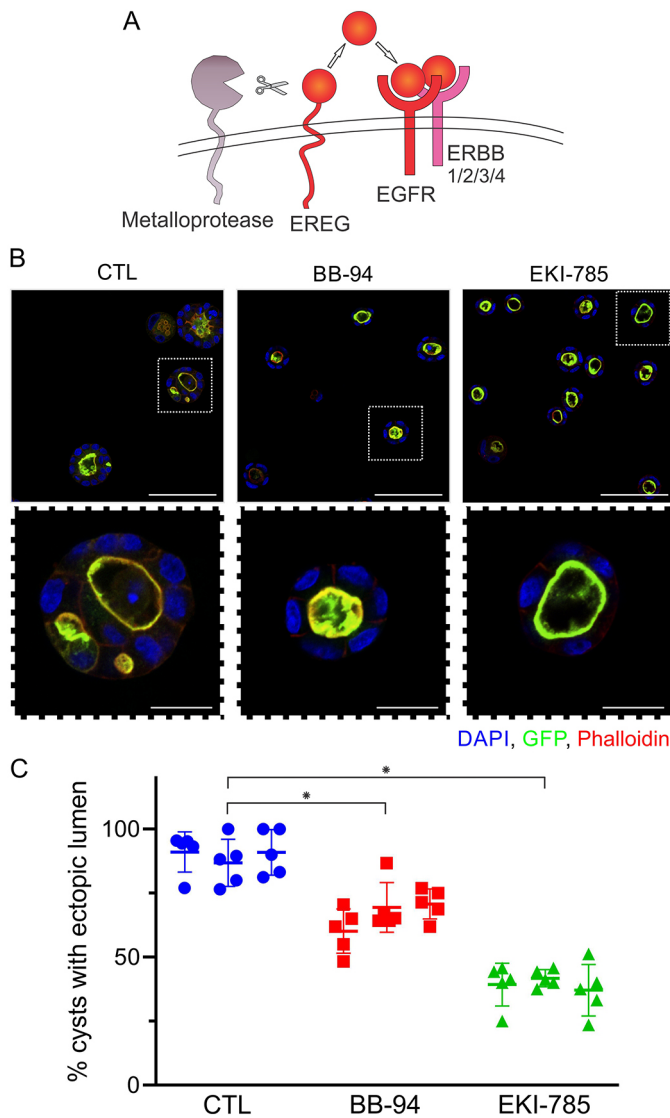


Fig. 6. Ectopic lumen formation is dependent on metalloprotease activity and EGFR signaling. (A) Metalloproteases cleave the EREG membrane precursor to release soluble EREG that then diffuses and binds to EGFR leading to its activation and downstream signaling. (B) MDCK cysts were induced for (Y156A)EREG–EGFP expression at day 3 and incubated with the metalloprotease inhibitor BB-94 (5 μ M) and the EGFR tyrosine kinase inhibitor EKI-785 (2 μ M). Cysts were fixed at day 6 and stained for DNA (DAPI, blue) and F-actin (phalloidin, red); EREG–GFP fluorescence is depicted in green. A low magnification field to show multiple cysts are shown on top, while equatorial plane images of individual cysts are displayed underneath. Scale bars: 100 μ m (top panels); 50 μ m (bottom magnified insets). (C) Quantification of results in B. Five random areas from three wells for each condition were imaged; cysts with ectopic lumens were counted and expressed as a fraction of the total cysts within that field (mean \pm s.d.). * P <0.05 (two-tailed unpaired t -test).

mutant EREG–EGFP chimera act as biologically active substrates for metalloprotease cleavage and biosynthetic trafficking. However, the most striking difference between WT and Y156A EREG still remains their delivery to opposite cell surfaces.

Ectopic lumen formation seen upon induction of EREG mistrafficking

EREG apical mistrafficking is associated with *in vivo* transformation and local invasion (Singh et al., 2013), and upon closer inspection,

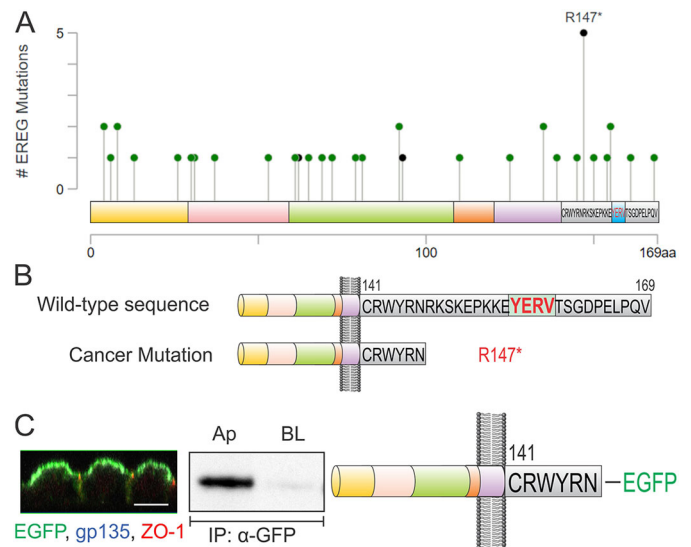


Fig. 7. The most common EREG cancer mutation leads to its apical mistrafficking in engineered MDCK cells. (A) EREG mutations in human cancers (<https://www.cbioportal.org>). Green markers indicate missense mutations and black markers indicate truncating mutations; marker height indicates mutation frequency. (B) The most common EREG human cancer mutation R147* (premature stop) removes the downstream EREG basolateral sorting motif. (C) Left panel, MDCK cells stably expressing (R147*)EREG–EGFP were fixed and immunostained for ZO-1 (red) and gp135 (blue). Confocal projections in xz planes are shown. Scale bar: 10 μ m. Middle panel, selective cell surface biotinylation of polarized MDCK cells stably expressing (R147*)EREG–EGFP labeled on apical (Ap) and basolateral (BL) cell surfaces. Images are representative of three repeats.

we observed structures resembling multiple lumens in MDCK xenografts (Fig. S2) and Matrigel cultures (Fig. 2) expressing apical EREG. 3D cultures predict *in vivo* behavior better than 2D plastic cultures, and the 3D ectopic lumen phenotype is associated with oncogenic perturbations in multiple epithelial cultures (Aranda et al., 2006; Li et al., 2014; Martin et al., 2008; Simian and Bissell, 2017). We thus define a MDCK multiple lumen phenotype in Matrigel as a surrogate for *in vivo* transformation.

Apical EREG disrupts a preformed epithelium

MDCK cells were seeded as a single-cell suspension in Matrigel and, after the first cell division, the two-cell stage cysts exhibited inverted polarity with the apical surface facing outward (Bryant et al., 2010). As cysts mature, apical proteins accumulate at the cell–cell interface at the region termed the apical membrane initiation site (AMIS), which expands and matures to become a single central lumen that is maintained through subsequent symmetric cell divisions. This process involves PKC β II-mediated phosphorylation of the gp135–NHERF1–ezrin complex, and inhibition of this pathway leads to formation of ectopic lumens (Bryant et al., 2014). Other proteins like Rab11, FIP5, cingulin and IRSp53 have been shown to ensure a single-lumen phenotype, while the cancer-promoting PRL-3 has been shown to induce multiple lumens (Bisi et al., 2020; Lujan et al., 2016; Mangan et al., 2016). After observing ectopic lumens with constitutive apical EREG expression (Fig. 2), we adopted inducible EREG expression to show that induction of apical EREG expression after formation of differentiated cysts after 3 days of culture is necessary and sufficient for loss of the single lumen phenotype (Fig. 3).

Differential effects of mistrafficked ERBB ligands in disruption of epithelial polarity

We previously determined that a small but signaling-competent pool of apical EGFR exists (Singh et al., 2013). We observed that basolateral addition of EREG to polarized MDCK cells led to the expected robust yet transient EGFR phosphorylation. In contrast, apical EREG addition led to weak but sustained EGFR phosphorylation (Singh et al., 2013). An apical pool of EGFR and apical EREG mutants could thus potentially establish a novel apical signaling platform that contributes to disruption of selective aspects of epithelial polarity.

We previously showed that mistrafficking of the EGFR ligand BTC in MDCK Transwell cultures was accompanied with additional apical structures at the cell–cell interface, which we termed lateral lumens, that resembled a hepatic polarity phenotype (Singh et al., 2015). Appearance of lateral lumens upon BTC mistrafficking showed that MDCK Transwell cultures deviated from columnar polarity and exhibited features of hepatic polarity (Cohen et al., 2004). These lateral lumens were typically observed between two adjacent cells. No lateral lumens were observed with apical EREG expression in MDCK Transwell cultures. Lateral lumens associated with BTC mistrafficking were typically restricted within two adjacent cells and were smaller than EREG-associated ectopic lumens, which may incorporate limiting membranes from multiple adjacent cells (Movie 1). Both ectopic and lateral lumen phenotypes were dependent on EGFR activity. BTC-induced EGFR signaling has previously been shown to control apicobasolateral polarity by regulating apical lumen size (Lof-Ohlin et al., 2017). Additionally, of the five EGFR ligands studied, only mistrafficking of EREG and BTC alters epithelial polarity, with both ligands incidentally also binding to ERBB4 (Komurasaki et al., 1997; Riese et al., 1996). ERBB4 may be involved in modulating epithelial polarity through these ligands. Interestingly, ERBB4 also has been shown to regulate polarity and lumen diameter during kidney development (Veikkolainen et al., 2012). It is interesting to speculate that cell–cell adhesion pathways that modulate columnar versus hepatic polarity may be differentially affected by BTC and EREG (Lazaro-Dieguez and Musch, 2017). Studying ligand-specific polarity alterations may thus enhance our understanding of the EGFR axis in epithelial polarity.

Potential mechanisms of ectopic lumen formation

Below we speculate on two potential mechanisms of multiple lumen phenotype that may involve EREG: (1) apoptosis regulation, and (2) regulation of the epithelial mitotic division plane. Usually a luminal environment is pro-apoptotic, in part, due to a lack of pro-survival ligands and luminal cells undergoing apoptosis after detaching from the extracellular matrix (Debnath et al., 2002). Apical EREG released into the lumen might suppress luminal cell apoptosis and lead to an incomplete lumen clearance and/or multiple lumens. Regulation of correct mitotic spindle orientation is a critical step in establishment and maintenance of epithelial polarity; cell division out of plane would lead to a loss of apicobasolateral polarity. EGFR signaling has been shown to regulate mitotic spindle orientation during symmetric cell division in epithelial cells (via IQGAP1 and NuMA) and asymmetric cell division in stem cells (via Aurora kinase A) (Banon-Rodriguez et al., 2014; Wang et al., 2019). In studies involving MDCK Matrigel cultures, EGFR ensured basolateral IQGAP1 localization, and loss of this interaction led to a non-polarized distribution of NuMA, loss of symmetric division and formation of multiple lumens (Banon-Rodriguez et al., 2014). Aberrant activation of EGFR by apical

EREG could thus also induce asymmetric division, leading to a multiple lumen phenotype. Thus, luminal apoptosis and regulated cell division could both be impacted by the EGFR signaling activated by apical EREG and result in a loss of epithelial polarity.

EREG is overexpressed in a number of cancers where its increased expression confers a metastatic phenotype and responsiveness to the EGFR-directed therapeutic cetuximab (Gupta et al., 2007; Jacobs et al., 2009; Khambata-Ford et al., 2007). We showed that the most common EREG mutation in cancer leads to its apical mistrafficking (Fig. 7). Apical EREG mistrafficking could additionally occur through the loss of a basolateral sorting adaptor that remains to be identified. Loss of polarity usually occurs early in cancer and is generally considered a consequence of transformation. Our work, however, shows that aberrant activation of EGFR signaling via apical EREG mistrafficking is sufficient to disrupt selective aspects of epithelial polarity.

MATERIALS AND METHODS

Reagents and antibodies

All chemicals were purchased from Sigma Chemical Co. (St. Louis, MO) unless otherwise stated. Galardin was purchased from Calbiochem (La Jolla, CA). BB-94 was purchased from R&D Systems Inc. (Minneapolis, MN). EZ-Link Sulfo-NHS-LC-Biotin was purchased from Pierce Biotechnology (Rockford, IL). BB-94, EK1-785, and galardin were prepared as 1–10 mM stocks in anhydrous DMSO and stored as small aliquots (50–100 μ l) at -20°C . Each aliquot was thawed immediately before use and was promptly refrozen after diluting; each aliquot was typically reused 2–5 times. All cell culture reagents were purchased from Gibco Laboratories (Grand Island, NY). Fluorescent secondary antibodies were purchased from Jackson ImmunoResearch Laboratories, Inc. (West Grove, PA). Protein G–agarose and rhodamine–phalloidin were purchased from Invitrogen (Carlsbad, CA). Rabbit polyclonal GFP (Cat #A-11120) and ZO-1 (Cat #61-7300) antibodies were purchased from Invitrogen. GFP antibodies were used at 1:2000 (1 $\mu\text{g}/\text{ml}$) for western blots and 2 μg (1 μl) for immunoprecipitation. ZO-1 antibodies were used at 1:600 dilution for immunofluorescence (0.25 mg/ml stock). Ezrin antibody was purchased from Cell Signaling Technology (Cat #3145) and was used at a dilution of 1:200. Acetylated tubulin antibody was purchased from Sigma (Cat #T6793) and was used at a dilution of 1:1500. The gp135 mouse monoclonal antibody was obtained as a gift from James R. Goldenring (Vanderbilt University Medical Center, Nashville, TN, USA) and was used at a dilution of 1:200.

Cell culture

Parental MDCK-II cells were obtained from Enrique Rodriguez-Boulan (Weill Cornell Medical College, Department of Ophthalmology, New York, NY, USA) (Dempsey and Coffey, 1994; Gravotta et al., 2007) and were maintained in Dulbecco's modified Eagle's medium (DMEM) containing 10% bovine growth serum (BGS), 0.1 mM non-essential amino acids, 2 mM L-glutamine and 100 U/ml penicillin/streptomycin.

Polarized epithelial cell culture

MDCK cells (100,000 in 0.5 ml) as a single-cell suspension were seeded on the inner chamber of 12 mm Transwell filters (polycarbonate, 0.4 μm pore size, Corning) in DMEM (10% BGS); 1.5 ml of medium was added to outer chambers. Fresh medium was replenished in inner and outer chambers every other day. Cells were considered polarized when the transepithelial electrical resistance (TEER) reached 200 Ω/cm^2 as described previously (Singh et al., 2015).

3D MDCK Matrigel culture

MDCK cells were split the day before starting the 3D Matrigel culture and Matrigel was put on ice for thawing overnight. On the day of culture, cells were trypsinized and reconstituted at a concentration of 1,000,000 cells/ml. Matrigel culture medium composition was DMEM with 0.1 mM non-essential amino acids, 2 mM L-glutamine and 100 U/ml penicillin/streptomycin, 5% fetal calf serum and 2% Matrigel. Cold Matrigel (5 μl)

was added to each well of cold eight-well chamber slides with cover glass bottom, and spread with glass capillaries with sealed tips. Matrigel was allowed to solidify for 5 min in the humidified incubator and 4000 cells were added to each well in a 200 μ l volume. Typically, 3 days after seeding, EREG expression was induced by addition of another 200 μ l of Matrigel culture medium containing doxycycline or inhibitors as needed. 3D cultures were maintained for an additional 2–5 days with medium replenished every 2–3 days.

EREG cloning and expression

WT and Y156A EREG–EGFP (constitutive) cloning has been described before (Singh et al., 2013). Other mutations and chimeras (truncations and substitutions) were subsequently derived from this construct. Doxycycline-inducible constructs were generated using the Gateway cloning system and pINDUCER20 plasmid obtained from Stephen J Elledge (Department of Genetics, Harvard Medical School, Boston, MA, USA) (Meerbrey et al., 2011). After 10–14 days of selection (300 μ g/ml G418) following viral induction, individual GFP-positive MDCK cells were cloned by FACS in 96-well dishes. Individual clones were allowed to grow and tested for their leakiness by western blotting for EREG–EGFP expression with or without addition of doxycycline. Clones with tight expression control (i.e. that only showed expression upon doxycycline addition) were used for subsequent studies. To maintain tight control of inducible clones, low-doxycycline/tetracycline serum was used. Clones were maintained in G418 (300 μ g/ml), which was removed during the experiments unless otherwise stated.

Cell lysis, immunoprecipitation and immunoblotting

For Transwell cultures, filters were cut out of the inserts and put in Eppendorf tubes containing 500 μ l of lysis buffer with the following composition: 50 mM HEPES (pH 7.5), 150 mM NaCl, 1% Triton X-100, 1 mM EDTA, 10% glycerol, 10 mM sodium pyrophosphate. Additionally, 2 mM sodium orthovanadate, 10 mM sodium fluoride, 1 mM PMSF, 5 μ g/ml leupeptin, 5 μ g/ml pepstatin, and 10 μ g/ml aprotinin were added just before lysis. Lysis was performed for 30 min at 4°C while rotating and then lysates were centrifuged (Sorvall Legend Micro 21R) at 16,000g for 15 min at 4°C for preclearing and lysates were subjected to immunoprecipitation and/or western blotting as described before (Singh et al., 2015).

Selective cell-surface biotinylation

We performed cell surface biotinylation as previously described selective (Singh et al., 2015). Briefly, 100,000 MDCK cells were allowed to polarize on 12 mm Transwell filters for ~6 days and were then washed with cold PBS supplemented with 0.1 mM CaCl₂ and 1.0 mM MgCl₂ (PBS-CM). EZ-Link Sulfo-NHS-LC-Biotin (0.5 mg/ml in cold PBS-CM) was then added either to the apical or basolateral compartments twice for 20 min. The biotinylation reaction was quenched by washing filters with PBS-CM containing 0.2% BSA and 100 mM glycine at 4°C. Filters were then cut out of the Transwell inserts and lysed and used for GFP immunoprecipitation and Western blotting.

Metabolic labeling and pulse-chase experiments on Transwell filters

500,000 MDCK cells expressing EREG constructs were allowed to polarize on 24 mm Transwell filters for ~6 days. Cells were then washed three times with L-cysteine- and L-methionine-free DMEM. [³⁵S]-Translabel (Met-Cys) was purchased from ICN Biomedicals (Costa Mesa, CA) and used at a concentration of 1 mCi/ml in L-cysteine- and L-methionine-free DMEM. 100 μ l puddles of label medium were placed on Parafilm and filters were placed on top and incubated for 20 min at 37°C in a humidified chamber. The label was then washed with DMEM with 10% bovine growth serum (BGS) containing 10 times excess L-cysteine and L-methionine at 18°C, and then chased with DMEM with BGS for the indicated times at 37°C. The chase was stopped by chilling cells in PBS (0.2% BSA) and filters were cut out of Transwell inserts and lysed and processed for immunoprecipitation for GFP as described above and run on SDS-PAGE (8–12% gradient) gels, fixed, dried, and exposed to capture radiolabeled EREG isoforms on autoradiography films as described previously (Singh et al., 2013).

Immunofluorescence and confocal microscopy

MDCK Matrigel cultures were fixed with 4% paraformaldehyde (PFA) for 5 min at room temperature while MDCK Transwell cultures were fixed with 4% PFA in PBS for 30 min at 4°C. Cells were then washed three times with cold PBS, and permeabilized in immunofluorescence buffer (IF buffer, 0.1% BSA, 0.1% Triton X-100 in PBS) overnight at 4°C as described previously (Singh et al., 2015). All subsequent steps were carried out at room temperature in IF buffer. Permeabilized cells were blocked with 5% normal donkey serum for 1 h, followed by incubation with primary antibody for 1 h. Excess primary antibody was removed by three washes with IF buffer (15 min each) and subsequently incubated with secondary antibody for 1 h. Samples were then washed three times with IF buffer (15 min each). Matrigel cultures were then covered in 300 μ l IF buffer and imaged within the next 2 days; Transwell inserts were then cut out and mounted in Prolong Gold mounting medium. Laser Scanning Confocal microscopy was performed using Nikon A1R inverted confocal microscope. Samples were scanned using 60X objective with Z slices taken at every 0.5 μ m intervals and images were analyzed using the NIS-Elements software. Images were subsequently processed using Adobe Photoshop or Corel PhotoPaint.

Electron microscopy

MDCK cysts were grown for 6 days on chamber slides and were then washed with PBS and fixed in their culture dishes with 2.5% glutaraldehyde in 0.1 M cacodylate. After fixation, the samples were gently lifted with the supporting Matrigel and postfixation in 1% OsO₄ for 1 h, enblock stained with 1% uranyl acetate for 30 min, and dehydrated with a graded ethanol series. Samples were infiltrated with Quetol 651 based Spurr's resin (Electron Microscopy Sciences) using propylene oxide as the transition solvent. The resin was polymerized at 60°C for 72 h, sectioned at 70 nm using a Leica UC7 Ultramicrotome and collected on copper slot grids. Samples were imaged on a Tecnai T12 at 100 kV using an AMT CCD camera.

Cell Titer Glo assay

Breast cancer cell line, HDQ-P1 was seeded in 96-well plate (10,000 cells/well) in 100 μ l volume with indicated concentrations of the EGFR neutralizing antibody, cetuximab, in quadruplicates. Fifty microliters of CellTiter-Glo assay reagent was added after 3 days of drug incubation and incubated for 30 min while shaking on an orbital shaker. Luminescence from the assay was measured using BioTek Synergy 4 plate reader.

Statistical analysis

Analysis was conducted in R software (<https://www.r-project.org/>) and figures were produced using ggplot2 (Villanueva et al., 2016), ggsci (ggsci: scientific journal and sci-fi themed color palettes for 'ggplot2' R package version 2.9), and ggpubr (ggpubr: 'ggplot2' Based Publication Ready Plots, version 0.3.0) packages. Differences in distributions were tested used the non-parametric Wilcoxon rank sum test and were considered statistically significant if $P < 0.05$.

Acknowledgements

We acknowledge the support of Vanderbilt University's Cell Imaging, Translational Pathology, and Flow Cytometry Shared Resources. We thank James R. Goldenring (Vanderbilt University) for the gp135 mouse monoclonal antibody. We thank Sarah E. Glass for editing the manuscript. We acknowledge support from the Nicholas Tierney GI Cancer Memorial Fund.

Competing interests

The authors declare no competing or financial interests.

Author contributions

Conceptualization: B.S., R.J.C.; Methodology: B.S., G.B., E.K., E.T.M., S.H., K.L.R., J.N.H., R.J.C.; Software: E.T.M.; Validation: B.S.; Formal analysis: B.S., G.B., E.K., E.T.M., S.H., K.L.R., J.N.H., R.J.C.; Investigation: B.S., G.B., E.K., S.H., K.L.R., J.N.H.; Resources: B.S., G.B., E.K., S.H., K.L.R., J.N.H.; Data curation: B.S., G.B., E.K., S.H., K.L.R.; Writing - original draft: B.S., E.K., K.L.R., R.J.C.; Writing - review & editing: B.S., E.K., K.L.R., R.J.C.; Visualization: B.S., E.T.M.; Supervision: B.S., R.J.C.; Project administration: B.S., R.J.C.; Funding acquisition: B.S., R.J.C.

Funding

This work was supported by National Institutes of Health grants NCI CA248505-01A1 (to B.S.), NCI P50 CA095103 (to R.J.C.), R35 CA197570 (to R.J.C.), and American Cancer Society Research Scholar Grant RSG-20-130-01-DDC (to B.S.). B.S. was supported by the GI SPORE Career Enhancement Program grant (NCI P50 CA095103) and the Vanderbilt Clinical and Translational Scholars Program (KL2TR002245). Deposited in PMC for release after 12 months.

Peer review history

The peer review history is available online at <https://journals.biologists.com/jcs/article-lookup/doi/10.1242/jcs.255927>

References

- Aranda, V., Haire, T., Nolan, M. E., Calarco, J. P., Rosenberg, A. Z., Fawcett, J. P., Pawson, T. and Muthuswamy, S. K. (2006). Par6-aPKC uncouples ErbB2 induced disruption of polarized epithelial organization from proliferation control. *Nat. Cell Biol.* **8**, 1235–1245. doi:10.1038/ncb1485
- Arteaga, C. L. and Engelman, J. A. (2014). ERBB receptors: from oncogene discovery to basic science to mechanism-based cancer therapeutics. *Cancer Cell.* **25**, 282–303. doi:10.1016/j.ccr.2014.02.025
- Banon-Rodriguez, I., Galvez-Santisteban, M., Vergara-Jauregui, S., Bosch, M., Borreguero-Pascual, A. and Martin-Belmonte, F. (2014). EGFR controls IQGAP basolateral membrane localization and mitotic spindle orientation during epithelial morphogenesis. *EMBO J.* **33**, 129–145. doi:10.1002/embj.201385946
- Bernascone, I., Hachimi, M. and Martin-Belmonte, F. (2017). Signaling networks in epithelial tube formation. *Cold Spring Harbor Perspect. Biol.* **9**, a027946. doi:10.1101/cshperspect.a027946
- Bhidi, G. P. and Colley, K. J. (2017). Sialylation of N-glycans: mechanism, cellular compartmentalization and function. *Histochem. Cell Biol.* **147**, 149–174. doi:10.1007/s00418-016-1520-x
- Bisi, S., Marchesi, S., Rizvi, A., Carra, D., Beznoussenko, G. V., Ferrara, I., Deflorian, G., Mironov, A., Bertalot, G., Pisati, F. et al. (2020). IRSp53 controls plasma membrane shape and polarized transport at the nascent lumen in epithelial tubules. *Nat. Commun.* **11**, 3516. doi:10.1038/s41467-020-17091-x
- Britain, C. M., Holdbrooks, A. T., Anderson, J. C., Willey, C. D. and Bellis, S. L. (2018). Sialylation of EGFR by the ST6Gal-I sialyltransferase promotes EGFR activation and resistance to gefitinib-mediated cell death. *J. Ovarian Res.* **11**, 12. doi:10.1186/s13048-018-0385-0
- Bryant, D. M., Datta, A., Rodriguez-Fraticelli, A. E., Peranen, J., Martin-Belmonte, F. and Mostov, K. E. (2010). A molecular network for de novo generation of the apical surface and lumen. *Nat. Cell Biol.* **12**, 1035–1045. doi:10.1038/ncb2106
- Bryant, D. M., Roignot, J., Datta, A., Overeem, A. W., Kim, M., Yu, W., Peng, X., Eastburn, D. J., Ewald, A. J., Werb, Z. et al. (2014). A molecular switch for the orientation of epithelial cell polarization. *Dev. Cell* **31**, 171–187. doi:10.1016/j.devcel.2014.08.027
- Cohen, D., Rodriguez-Boulant, E. and Musch, A. (2004). Par-1 promotes a hepatic mode of apical protein trafficking in MDCK cells. *Proc. Natl. Acad. Sci. USA* **101**, 13792–13797. doi:10.1073/pnas.0403684101
- Debnath, J., Mills, K., Collins, N., Reginato, M., Muthuswamy, S. and Brugge, J. (2002). The role of apoptosis in creating and maintaining luminal space within normal and oncogene-expressing mammary acini. *Cell* **111**, 29–40. doi:10.1016/S0092-8674(02)01001-2
- Dempsey, P. J. and Coffey, R. J. (1994). Basolateral targeting and efficient consumption of transforming growth factor- α when expressed in Madin-Darby canine kidney cells. *J. Biol. Chem.* **269**, 16878–16889. doi:10.1016/S0021-9258(19)89472-3
- Dempsey, P. J., Meise, K. S., Yoshitake, Y., Nishikawa, K. and Coffey, R. J. (1997). Apical enrichment of human egf precursor in madin-darby canine kidney cells involves preferential basolateral ectodomain cleavage sensitive to a metalloprotease inhibitor. *J. Cell Biol.* **138**, 747–758. doi:10.1083/jcb.138.4.747
- Dempsey, P. J., Meise, K. S. and Coffey, R. J. (2003). Basolateral sorting of transforming growth factor- α precursor in polarized epithelial cells: characterization of cytoplasmic domain determinants. *Exp. Cell Res.* **285**, 159–174. doi:10.1016/S0014-4827(03)00035-1
- Gao, J., Aksoy, B. A., Dogrusoz, U., Dresdner, G., Gross, B., Sumer, S. O., Sun, Y., Jacobsen, A., Sinha, R., Larsson, E. et al. (2013). Integrative analysis of complex cancer genomics and clinical profiles using the cBioPortal. *Sci. Signal.* **6**, 11. doi:10.1126/scisignal.6273er1
- Gephart, J. D., Singh, B., Higginbotham, J. N., Franklin, J. L., Gonzalez, A., Folsch, H. and Coffey, R. J. (2011). Identification of a novel mono-leucine basolateral sorting motif within the cytoplasmic domain of amphiregulin. *Traffic* **12**, 1793–1804. doi:10.1111/j.1600-0854.2011.01282.x
- Gravotta, D., Deora, A., Perret, E., Oyanadel, C., Soza, A., Schreiner, R., Gonzalez, A. and Rodriguez-Boulant, E. (2007). AP1B sorts basolateral proteins in recycling and biosynthetic routes of MDCK cells. *Proc. Natl. Acad. Sci. USA* **104**, 1564–1569. doi:10.1073/pnas.0610700104
- Groenesteghe, W. M., Thebault, S., van der Wijst, J., van den Berg, D., Janssen, R., Tejpar, S., van den Heuvel, L. P., van Cutsem, E., Hoenderop, J. G., Knoers, N. V. et al. (2007). Impaired basolateral sorting of pro-EGF causes isolated recessive renal hypomagnesemia. *J. Clin. Invest.* **117**, 2260–2267. doi:10.1172/JCI31680
- Gupta, G., Nguyen, D., Chiang, A., Bos, P., Kim, J., Nadal, C., Gomis, R., Manova-Todorova, K. and Massague, J. (2007). Mediators of vascular remodelling co-opted for sequential steps in lung metastasis. *Nature* **446**, 765–770. doi:10.1038/nature05760
- Harris, R. C., Chung, E. and Coffey, R. J. (2003). EGF receptor ligands. *Exp. Cell Res.* **284**, 2–13. doi:10.1016/S0014-4827(02)00105-2
- Hobert, M. and Carlin, C. (1995). Cytoplasmic juxtamembrane domain of the human EGF receptor is required for basolateral localization in MDCK cells. *J. Cell. Physiol.* **162**, 434–446. doi:10.1002/jcp.1041620316
- Hobert, M. E., Kil, S. J., Medof, M. E. and Carlin, C. R. (1997). The cytoplasmic juxtamembrane domain of the epidermal growth factor receptor contains a novel autonomous basolateral sorting determinant. *J. Biol. Chem.* **272**, 32901–32909. doi:10.1074/jbc.272.52.32901
- Jacobs, B., De Roock, W., Piessevaux, H., Van Oirbeek, R., Biesmans, B., De Schutter, J., Fieuws, S., Vandesompele, J., Peeters, M., Van Laethem, J. L. et al. (2009). Amphiregulin and epiregulin mRNA expression in primary tumors predicts outcome in metastatic colorectal cancer treated with cetuximab. *J. Clin. Oncol.* **27**, 5068–5074. doi:10.1200/JCO.2008.21.3744
- Khambata-Ford, S., Garrett, C. R., Meropol, N. J., Basik, M., Harbison, C. T., Wu, S., Wong, T. W., Huang, X., Takimoto, C. H., Godwin, A. K. et al. (2007). Expression of epiregulin and amphiregulin and K-ras mutation status predict disease control in metastatic colorectal cancer patients treated with Cetuximab. *J. Clin. Oncol.* **25**, 3230–3237. doi:10.1200/JCO.2006.10.5437
- Komurasaki, T., Toyoda, H., Uchida, D. and Morimoto, S. (1997). Epiregulin binds to epidermal growth factor receptor and ErbB-4 and induces tyrosine phosphorylation of epidermal growth factor receptor, ErbB-2, ErbB-3 and ErbB-4. *Oncogene* **15**, 2841–2848. doi:10.1038/sj.onc.1201458
- Kuwada, S. K., Lund, K. A., Li, X. F., Clifton, P., Amsler, K., Opreko, L. K. and Wiley, H. S. (1998). Differential signaling and regulation of apical vs. basolateral EGFR in polarized epithelial cells. *Am. J. Physiol.* **275**, C1419–C1428. doi:10.1152/ajpcell.1998.275.6.C1419
- Lazaro-Dieguez, F. and Musch, A. (2017). Cell-cell adhesion accounts for the different orientation of columnar and hepatocytic cell divisions. *J. Cell Biol.* **216**, 3847–3859. doi:10.1083/jcb.201608065
- Li, Y., Xu, J., Xiong, H., Ma, Z., Wang, Z., Kipreos, E. T., Dalton, S. and Zhao, S. (2014). Cancer driver candidate genes AVL9, DENND5A and NUPL1 contribute to MDCK cystogenesis. *Oncoscience* **1**, 854–865. doi:10.18632/oncoscience.107
- Lof-Ohlin, Z. M., Nyeng, P., Bechard, M. E., Hess, K., Bankaitis, E., Greiner, T. U., Ameri, J., Wright, C. V. and Semb, H. (2017). EGFR signalling controls cellular fate and pancreatic organogenesis by regulating apicobasal polarity. *Nat. Cell Biol.* **19**, 1313–1325. doi:10.1038/ncb3628
- Lujan, P., Varsano, G., Rubio, T., Hennrich, M. L., Sachsenheimer, T., Galvez-Santisteban, M., Martin-Belmonte, F., Gavin, A. C., Brugger, B. and Kohn, M. (2016). PRL-3 disrupts epithelial architecture by altering the post-mitotic midbody position. *J. Cell Sci.* **129**, 4130–4142.
- Mangan, A. J., Sietsema, D. V., Li, D., Moore, J. K., Citi, S. and Prekeris, R. (2016). Cingulin and actin mediate midbody-dependent apical lumen formation during polarization of epithelial cells. *Nat. Commun.* **7**, 12426. doi:10.1038/ncomms12426
- Martin-Belmonte, F. and Mostov, K. (2008). Regulation of cell polarity during epithelial morphogenesis. *Curr. Opin. Cell Biol.* **20**, 227–234. doi:10.1016/j.cceb.2008.01.001
- Martin, K. J., Patrick, D. R., Bissell, M. J. and Fournier, M. V. (2008). Prognostic breast cancer signature identified from 3D culture model accurately predicts clinical outcome across independent datasets. *PLoS ONE* **3**, e2994. doi:10.1371/journal.pone.0002994
- Meerbrey, K. L., Hu, G., Kessler, J. D., Roarty, K., Li, M. Z., Fang, J. E., Herschukowitz, J. I., Burrows, A. E., Ciccio, A., Sun, T. et al. (2011). The pINDUCKER lentiviral toolkit for inducible RNA interference in vitro and in vivo. *Proc. Natl. Acad. Sci. USA* **108**, 3665–3670. doi:10.1073/pnas.1019736108
- Merchant, N. B., Voskresensky, I., Rogers, C. M., LaFleur, B., Dempsey, P. J., Graves-Deal, R., Revetta, F., Foutch, A. C., Rothenberg, M. L., Washington, M. K. et al. (2008). TACE/ADAM-17: a component of the epidermal growth factor receptor axis and a promising therapeutic target in colorectal cancer. *Clin. Cancer Res.* **14**, 1182–1191. doi:10.1158/1078-0432.CCR-07-1216
- Riese, D. J., 2nd, Bermingham, Y., van Raaij, T. M., Buckley, S., Plowman, G. D. and Stern, D. F. (1996). Betacellulin activates the epidermal growth factor receptor and erbB-4, and induces cellular response patterns distinct from those stimulated by epidermal growth factor or neuregulin-beta. *Oncogene* **12**, 345–353.
- Schluter, M. A. and Margolis, B. (2009). Apical lumen formation in renal epithelia. *J. Am. Soc. Nephrol.* **20**, 1444–1452. doi:10.1681/ASN.2008090949
- Simian, M. and Bissell, M. J. (2017). Organoids: a historical perspective of thinking in three dimensions. *J. Cell Biol.* **216**, 31–40. doi:10.1083/jcb.201610056
- Singh, B. and Coffey, R. J. (2014). Trafficking of epidermal growth factor receptor ligands in polarized epithelial cells. *Annu. Rev. Physiol.* **76**, 275–300. doi:10.1146/annurev-physiol-021113-170406

- Singh, B., Bogatcheva, G., Washington, M. K. and Coffey, R. J. (2013). Transformation of polarized epithelial cells by apical mistrafficking of epiregulin. *Proc. Natl. Acad. Sci. USA* **110**, 8960–8965. doi:10.1073/pnas.1305508110
- Singh, B., Bogatcheva, G., Starchenko, A., Sinnaeve, J., Lapierre, L. A., Williams, J. A., Goldenring, J. R. and Coffey, R. J. (2015). Induction of lateral lumens through disruption of a monoleucine-based basolateral-sorting motif in betacellulin. *J. Cell Sci.* **128**, 3444–3455.
- Veikkolainen, V., Naillat, F., Railo, A., Chi, L., Manninen, A., Hohenstein, P., Hastie, N., Vainio, S. and Elenius, K. (2012). ErbB4 modulates tubular cell polarity and lumen diameter during kidney development. *J. Am. Soc. Nephrol.* **23**, 112–122. doi:10.1681/ASN.2011020160
- Vermeer, P. D., Einwalter, L. A., Moninger, T. O., Rokhlina, T., Kern, J. A., Zabner, J. and Welsh, M. J. (2003). Segregation of receptor and ligand regulates activation of epithelial growth factor receptor. *Nature* **422**, 322–326. doi:10.1038/nature01440
- Villanueva, R., Chen, Z. and Wickham, H. (2016). *ggplot2: Elegant Graphics For Data Analysis Using The Grammar Of Graphics*. New York, NY: Springer-Verlag.
- Wang, H., Lacoche, S., Huang, L., Xue, B. and Muthuswamy, S. K. (2013). Rotational motion during three-dimensional morphogenesis of mammary epithelial acini relates to laminin matrix assembly. *Proc. Natl. Acad. Sci. U.S.A.* **110**, 163–168. doi:10.1073/pnas.1201141110
- Wang, Y. X., Feige, P., Brun, C. E., Hekmatnejad, B., Dumont, N. A., Renaud, J. M., Faulkes, S., Guindon, D. E. and Rudnicki, M. A. (2019). EGFR-Aurka signaling rescues polarity and regeneration defects in dystrophin-deficient muscle stem cells by increasing asymmetric divisions. *Cell Stem Cell* **24**, 419–432.e416. doi:10.1016/j.stem.2019.01.002